ORIGINAL PAPER

Main structural and mechanical properties of electrospun PAN-based carbon nanofibers as a function of carbonization maximum temperature

Mahdi Valinejad Qanati[1] · Ali Rasooli[1] · Mohammad Rezvani[1]

Abstract

In this study, PAN-based carbon nanofibers (CNFs) were synthesized via electrospinning followed by stabilizing and carbonization. The carbonization process was performed by heating the fibrous mats up to a maximum temperature in the region of 800–1600 °C. The effect of carbonization maximal temperature on the structure and tensile strength of carbon nanofiber mats was investigated via SEM, elemental analysis, X-ray diffraction, Raman spectroscopy and tensile testing. Polyacrylonitrile (PAN) concentrations of 6–10% (w/w) and voltages of 14–16 kV were recognized as the optimal electrospinning parameters in order to synthesize of nanofibrous mats without any agglomerated nanoparticles or beads in the mats structure. It is clear from the results that carbon content, crystalline stacking size (Lc), in-plane crystallite size (La) and the number of graphene layers in single crystallite continuously increased with rising carbonization maximum temperature from 800 to 1600 °C, while interlayer d-spacing (d_{002}) decreased at the maximum temperatures of 1000–1400 °C, firstly. This value increased again at the maximum temperatures above 1400 °C due to the formation of considerable shrinkages and pores in the CNFs structure. The highest value of tensile strength (206–223 MPa) was recorded for the CNFs mats carbonized up to 1200–1400 °C.

Keywords CNFs · PAN · DMF · Electrospinning · Carbonization · Poisson Ratio

✉ Ali Rasooli
 A.Rasooli@tabrizu.ac.ir

 Mahdi Valinejad Qanati
 Mvalinejad64@yahoo.com

 Mohammad Rezvani
 M_rezvani@tabrizu.ac.ir

1 Department of Materials Science and Engineering, Faculty of Mechanical Engineering, University of Tabriz, Tabriz, Iran

Introduction

Carbon fibers (CFs) and nanofibers (CNFs) are mainly applied to reinforce polymers, much like glass fibers have been used for decades in fiberglass reinforced polyesters, with the principal difference that composites with CFs are so-called advanced composites or high-performance composites. The progress achieved with CNFs, as compared with glass reinforcement fibers, is based on the superior stiffness of CNFs combined with high strength and low density [1]. Electrospinning is a simple, efficient, economical technique for the large-scale fabrication of concatenated nanofibers [2]. This technique is often used in the development of nanostructure fibers consisting of ceramics, metals and polymeric materials. Electrospinning has some inherent advantages and disadvantages. Advantages of this technique include the efficiency and simplicity of the procedure, the inexpensive setup, and the ability to control many factors, such as the fiber diameter, orientation, and composition; disadvantages include the use of organic solvents and the limited control of pore structures. In the case of ceramic nanofibers, control of pore structures of the synthesized fibers and its physical and mechanical properties can be performed during carbonization process [3]. Also, synthetic polymers are considerably easier than natural polymers to electrospin, which is reflected by the larger number of synthetic polymers that have been electrospun into nanofibers. Natural polymers are often blended with synthetic polymers or salts to increase the solution viscosity and consistency in electrospinning [2].

Recently, CNFs are mostly prepared via electrospinning followed by stabilizing and carbonization process [4]. Of the various precursors to synthesis of electrospun carbon fibers, polyacrylonitrile (PAN) has been the most commonly used due to its high carbon content [5]. Electrospinning of a PAN solution in a proper solvent such as dimethylsulphoxide (DMSO) or dimethylformamide (DMF) can lead to the polymeric fibers with diameters smaller than 1 μm [6–9]. Diameter of electrospun carbon fibers and its morphology is affected by many electrospinning parameters such as the solution properties and concentration, hydrostatic pressure in the capillary tube, the distance between the tip, collector and electric potential on the capillary tip and electrospinning voltage [10]. Stabilizing followed by carbonization is carried in order to convert polymeric PAN fibers to carbon fibers [6]. Stabilizing process involves the as-spun nanofibers heating up to the temperatures of 180–300 °C in the air atmosphere, that is performed to further cross-link the PAN molecules in order to prevent of the fibers decomposing at the high carbonization temperatures [11]. Carbonization process involves the as-spun nanofibers heating up to a maximal temperature above 800 °C in an inert atmosphere. This step is an aromatic growth and polymerization step in which the non-carbon elements are removed as volatile gases in the form of hydrogen, nitrogen, water, ammonia, etc. After carbonization process, the fibers diameter is reduced due to expulsion of non-carbon elements and leaving an amorphous carbon structure [12–14]. In fact, the carbon content of the carbonized fiber can range from 80% to in excess of 99%wt. depending on carbonization maximum temperature

(T_{max}) [15, 16]. Carbonized fibers consist of polyaromatic (graphite structure) and disordered carbons (turbostratic structure) that are shown in Fig. 1 [1].

Crystallite structure of CNFs is highly affected by T_{max} [17]. Crystallite more important parameters of CNFs are the crystalline stacking thickness or crystalline size (L_c), in-plane graphitic crystallite size (La) and interlayer d-spacing (d_{002}) that vary with the carbonization maximum temperature [18, 19]. These crystallite parameters can effect on the mechanical properties of carbonized CNFs. Therefore, it is important to investigate the T_{max} effect on the crystallite parameters in order to obtain high-performance CNFs with the good mechanical properties. Hence, the aim of the present investigation was to study the effects of the carbonized CNFs structure and chemical composition on the mechanical properties of CNFs mats. Firstly, the more effective electrospinning parameters (voltage and concentration of electrospinning solution) have been optimized in order to produce the fine and homogeneous carbon nano-sized fibers. The electrospun PAN nanofibers obtained from the electrospinning optimal conditions were selected to stabilizing and carbonization process. As-spun PAN nanofibers were firstly stabilized at 300 °C in the air atmosphere and then carbonized up to the various maximum temperatures in the region of 800–1600 °C. Finally, the structure and properties of the carbonized CNFs mats were characterized using the various analysis techniques including scanning electron microscopy (SEM), elemental analysis, X-ray diffraction, Raman spectroscopy and tensile testing in order to optimize the carbonization maximal temperature.
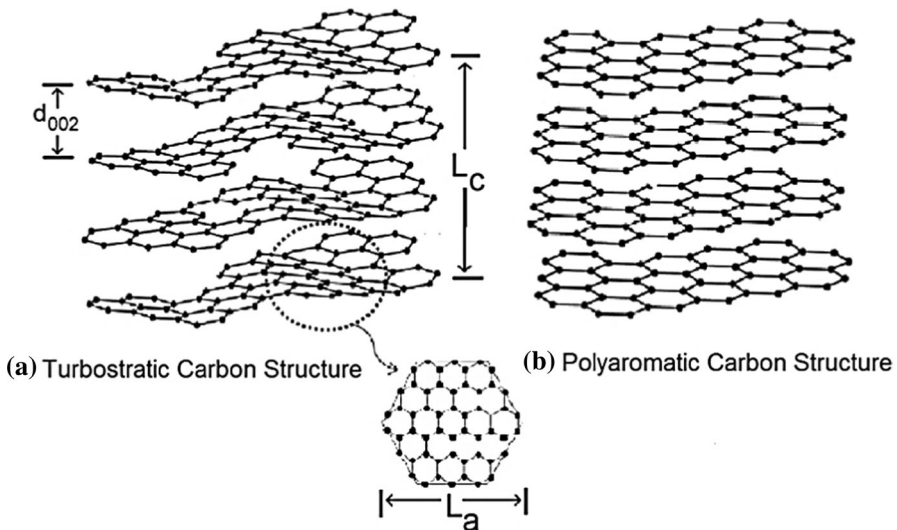

Fig. 1 Schematic of the carbon turbostratic (**a**) and polyaromatic structure (**b**)

Materials and methods

Materials

Materials including PAN and DMF were purchased from Sigma-Aldrich Co. Specifications of the materials are listed in Table 1.

Electrospinning and carbonization of PAN fibers

The electrospinning device used in this study was a horizontal type (Model ES-1000) produced by Fanavaran Nano-Meghyas Co. To improve PAN electrospinning feasibility, DMF was selected as a solvent to prepare electrospinning solution. To synthesize fine fibrous mats with homogenous morphology, PAN resin concentration in solution and electrospinning voltage underwent changes and optimized.

Firstly, to reach the optimal electrospinning voltage, a solution with 8% (w/w) concentration of PAN in DMF was spun at the applied voltages of 10, 12, 14, 16, and 18 kV. Average diameter of the samples electrospun by various electrospinning voltages was measured by imagining via scanning electron microscope (SEM) and the voltage range resulted in fibrous samples smaller than 500 nm (average diameter $\leq$ 500 nm without any bead and agglomerated particle) was recorded as the optimal voltage range. In the next step, the characteristic of PAN fiber web was considered with various concentrations of PAN in DMF (6, 8, 10, 12, 14 and 16% (w/w)) at the optimal applied voltage in order to optimize concentration of electrospinning solution. For each sample, electrospinning distance, injection flow rate and electrospinning time were 13 cm, 0.8 ml/h and 3 h, respectively. The nanofibrous mats were collected by a highly rotating disk covered by aluminum foil (diameter of 30 cm) with a linear speed of 24 m/s.

Stabilization and carbonization

After synthesize of electrospun PAN fibers, stabilizing of fibrous mat was performed in the air atmosphere followed by carbonization in a tubular furnace with cylindrical chamber of quartz, under constant flow of argon. Firstly, the sample was stabilized in air at 300 °C for 1 h and then was carbonized by heating from ambient temperature to a maximum temperature (T_{max}) in the region of 800–1600 °C (heating rate of 10 °C.min^{-1}). The effect of T_{max} on the morphology and structure of carbon nanofibers was studied, finally.

Table 1 Specifications of used materials for synthesize of electrospun fibers

Material	Synonym	CAS number	Chemical formula	Molecular mass (g.mol^{-1})
Polyacrylonitrile	PAN	25,014–41-9	$(C_3H_3N)_n$	53.06
Dimethylformamide	DMF	68–12-2	C_3H_7NO	73.09

Elemental analysis

The amounts of C, H, N, S and O in CNFs samples were measured by an elemental analyzer (Flash 2000, Thermo Scientific, USA). The elements of C, H, N and S were analyzed using oxygen and helium gas at 800 °C for 700 s. Oxygen was analyzed using helium gas at 1100 °C for 500 s.

Structural study

Morphological studies of the fibers were performed using LEO 440i SEM (England). Fibers average diameter was measured using image analysis software. To measure the average diameter of fibers, 30 fibers in the SEM micrograph were selected randomly and the average value of them was considered as the average diameter of fibers. XRD diffractometer (Siemens D5000) was used to investigate the crystalline structure of CNFs and calculate the L_C and interlayer spacing (d_{002}) by Cu K_α radiation ($\lambda = 1.54$ Å) in 2θ scan mode. The acceleration voltage and emission current were 45 kV and 200 mA, respectively. The 2θ value ranged from 10° to 40°. Raman scattering studies were performed via a micro-spectrometer (Takram P50C0R10, Teksan) by the use of a 488 nm excitation produced by an argon ion laser operating at 12 mW, in the range of 750–2250 cm^{-1}. The beam was focused on an area of 0.25 mm^2, and the scattered light was analyzed by the use of a 270 mm grating spectrometer.

The specific volume of Lennard–Jones potential of CNFs samples was calculated according to the Eq. (1) developed by M. Al-Raeei and M. S. El-Daher [20], where ε represents depth of the Lennard–Jones potential, k_B is Boltzmann constant (~ 0.002 kcal mol^{-1} K^{-1}), T is absolute temperature and v_0 is the volume of particles in the system. Particles volume (v_0) is approximately equal to d^3 ($v_0 \cong d^3$), where d is the diameter of carbon atoms. Finally, curves of the samples specific volume were depicted versus the temperature.

$$v_m = \sqrt{1 + \sqrt{1 + \left(\frac{k_B \cdot T}{\varepsilon}\right)}} \, v_0 \tag{1}$$

The specific surface area and pore volume of the samples were measured by means of N_2 adsorption at 77 °C using Brunauer–Emmett–Teller (BET Tristar II 3020 Micromeritics). Prior to adsorption, the samples were out-gassed under vacuum at 100 °C for 12 h. The specific surface area was calculated in the relative pressure interval of 0.04–0.2 using the Brunauer–Emmett–Teller method [21] The total pore volume (V_t) was given by the adsorption isotherm at the relative pressure P/P0 equal to 0.96 [22].

Tensile strength testing

The samples for mechanical testing were prepared by cutting the electrospun fibrous mats into rectangle shape with a size of 20×5 mm. Tensile tests were performed

by a computer-controlled electromechanical testing machine (CMT-8102, Shenzhen, China) at a stretching rate of 5 mm/min. Stress–strain curve of the samples was depicted by TRAPEZIUMX-V Materials Testing Software. Young's modulus (E) of the samples is obtained by measuring the slope of the axial stress–strain curve in the elastic region.

Results and discussion

Electrospinning and carbonization of PAN fibers

Figure 2 shows the SEM images of the acrylonitrile fibers that were spun from a solution with concentration of 8% (w/w) at the applied voltages of 12, 14 and 16 kV. As seen in Fig. 2a, at the voltage of 12 kV, electrical force was not enough to overcome the solution surface tension and therefore resulted in creation of large amount of PAN nanoparticles and very short fibers with average diameter of 820 nm.

There was not observed any impurity such as nanoparticle or bead in the structure of the samples that were spun at the voltages of 14 and16 kV (Fig. 2b, c). Fibers average diameter for the webs that were obtained at the voltages of 14 and 16 kV were 324 and 221 nm, correspondingly. At the voltages more than 16 kV, the electrical force was too high and so whipping movement of jet increased, significantly. Intensified whipping movement of jet increased electrospinning solution flow entanglement resulted in the unstable jet formation. Spinning jet formation was not observed at the voltage of 10 kV. Because of uniform and fine fibers formation without any bead and agglomerated particles, voltages of 14–16 kV were found out as the optimal voltage region.

Figure 3 shows the SEM micrographs for the acrylonitrile fiber webs that were spun from the solutions with concentration of 6–16% (w/w) at an optimal value of applied voltage (15 kV). Using image analysis software proved that concentration increasing leads to increase the fibers average diameter (Fig. 4). The significant increasing diameter was observed by increase of concentration above 10% (w/w). For the concentration above 10% (w/w), viscosity of the electrospinning solution increases to such an extent that the number of macromolecular chains as well as chain entanglements in the electrospinning solution increase, while the size of Taylor cone keeps relatively constant. Therefore, the charged jet becomes thicker, due to the higher viscosity resistance leading to the significant increase of fiber diameter. This value (10% w/w) could be recorded as the critical electrospinning concentration [23].

The average diameter value for the fibers that were spun from the solutions of 6, 8 and 10% (w/w) were reported as 205, 271 and 446 nm, correspondingly. Micro-sized fibers were spun for the concentrations of 12 and 14% (w/w). The average diameter value for the fibers synthesized from the solutions of 12 and 14% (w/w) was recorded 963 and 1245 nm, respectively. At concentration of 16% (w/w), electrical force was not enough to overcome the solution surface tension and therefore a large amount of agglomerated nanoparticles have been spun (Fig. 3f).
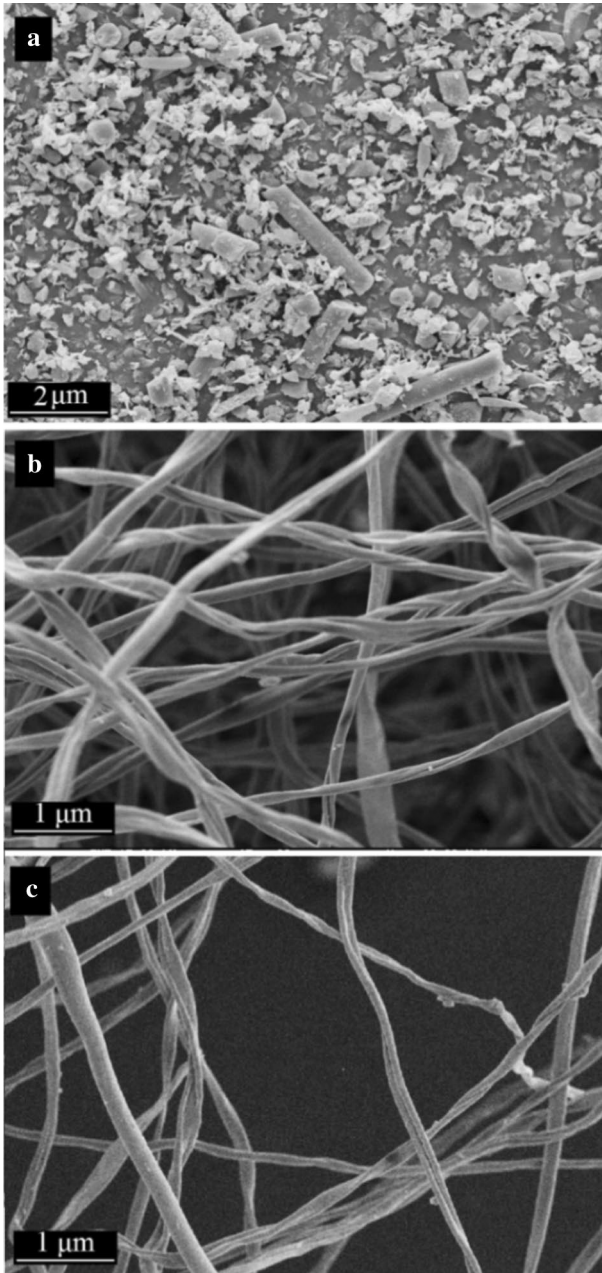
Fig. 2 SEM images of the acrylonitrile nanofibers that were spun from 8% (w/w) PAN in DMF at 12 kV (**a**), 14 kV (**b**) and 16 kV (**c**)
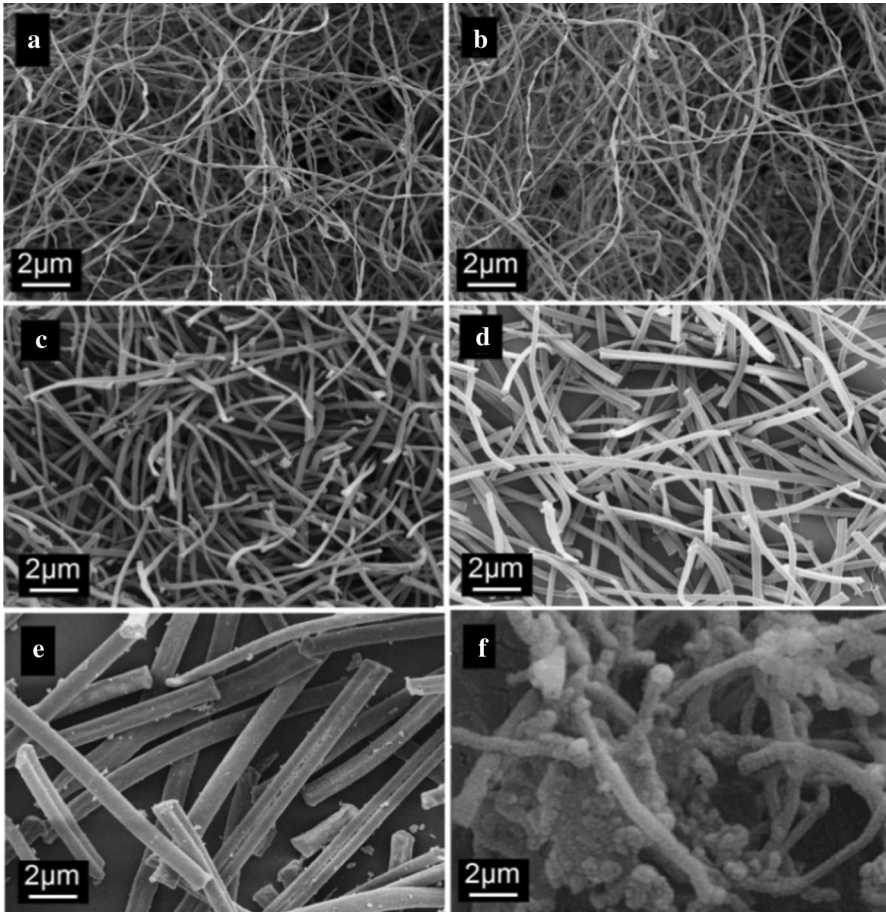
Fig. 3 SEM images of the PAN nanofibers that were spun from the solution of 6% (**a**), 8% (**b**), 10% (**c**), 12% (**d**), 14% and 16% (w/w) at 15 kV

Spinning jet formation was not observed at the concentrations more than 16% (w/w). Concentrations of 6–10% (w/w) were found out as the optimal PAN concentration range in order to synthesize of nano-sized fibers. The effect of electrospinning parameters on the average diameter of the fibers is summarized in Table 2.

Carbonization

PAN nanofibrous mat obtained from the electrospinning optimal parameters (PAN concentration of 6% (w/w) and electrospinning voltage of 15 kV) was stabilized and then carbonized up to a maximum temperature (T_{max}) in the region of 800–1600 °C (heating rate of 10 °C.min^{-1}). As seen in Table 3, carbon content (% C) of carbonized nanofibers continuously increased with the increase of T_{max}. The content of Nitrogen (% N), Oxygen (% O) and Hydrogen (% H) significantly decreases by
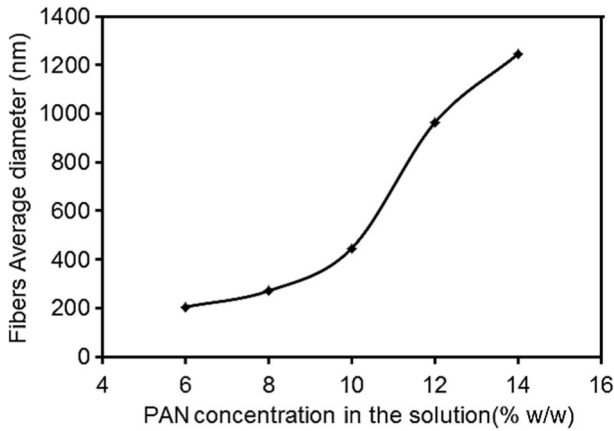
Fig. 4 Average diameter of electrospun fibers as a function of PAN concentration in the electrospinning solution

**Table 2** the average diameter of the nanofibers that were spun at the various electrospinning parameters

PAN concentration (% w/w)	Applied voltage (kV)	Fibers average diameter (nm)	Status
8	10	–	Spinning jet formation was not observed
8	12	820	Very short fibers with numerous nano-particle were spun
8	14	324	Successful
8	16	221	Successful
8	18	–	unstable jet formation
6	15	205	Successful
8	15	271	Successful
10	15	446	Successful
12	15	963	Micro-sized fibers were spun
14	15	1245	Micro-sized fibers were spun
16	15	–	Micro-sized fibers adhered together by agglomerated nanoparticles

Table 3 Elemental analysis of CNFs as a function of carbonization maximum temperature

T_{max} (°C)	C (%wt)	N (%wt)	H (%wt)	O (%wt)
800	79.42	9.93	3.11	7.54
1000	85.68	7.65	1.28	5.39
1200	90.53	5.51	0.47	3.49
1400	91.75	4.94	0	3.31
1600	92.87	4.15	0	2.98

increase of T_{max} from 800 °C to 1200 °C. This matter can decrease the fibers average diameter. For the nanofibers carbonized at the temperatures above 1200 °C, H was completely eliminated from fibers structure that confirms the number of C-H bond in the nanofibers structure is zero. N and O contents slightly decreased with the increase of T_{max} from 1200 to 1600 °C. It is expected that the more turbostratic structure change to graphite-like structure with the decrease of N and O content and so decrease of the non-carbon bond.

Figure 5 shows the SEM micrographs of the CNFs that were spun from the solutions of 6% (W/W) at 15 kV applied voltage followed by stabilizing at 300 ˚C and carbonization up to the temperatures of 800–1600 ˚C. It is clear from this figure and Fig. 6 that CNFs average diameter decreased with increase of T_{max} from 800 to 1200 ˚C. This is due to the decrease of N, O and H contents in the CNFs
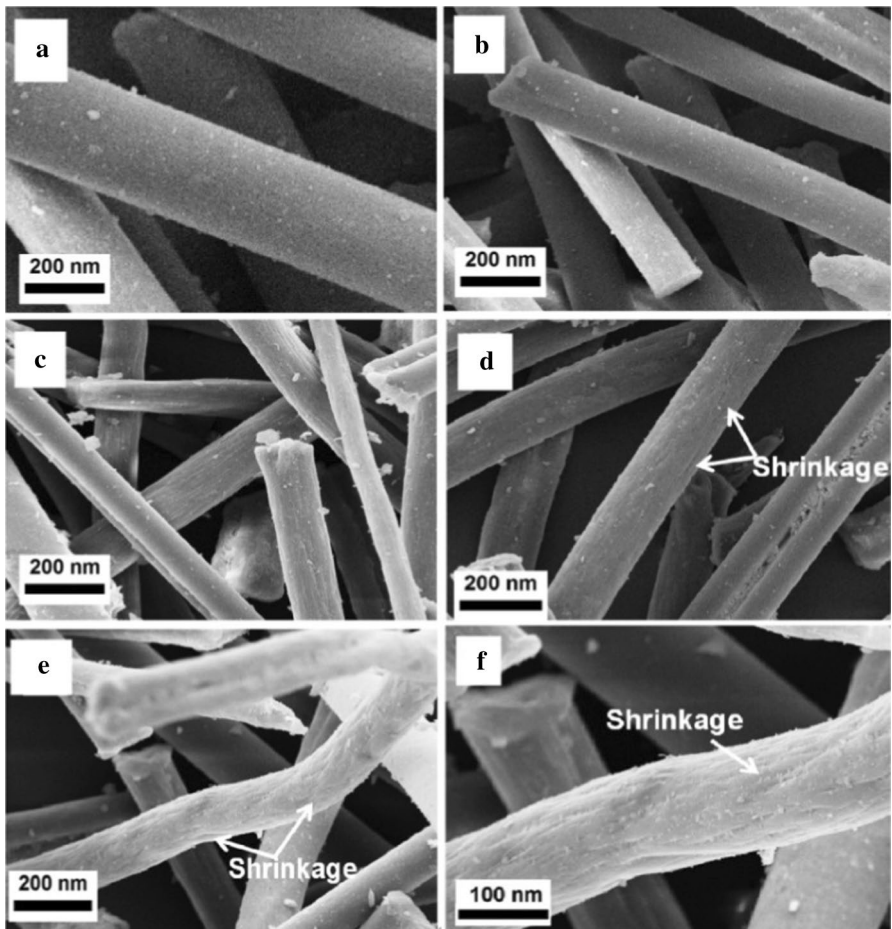
Fig. 5 SEM image of PAN-based CNFs carbonized up to 800 °C (**a**), 1000 °C (**b**), 1200 °C (**c**), 1400 °C (**d**), 1600 °C (magnification of 60 kX) (**e**) and 1600 °C (magnification of 100 kX) (**f**)
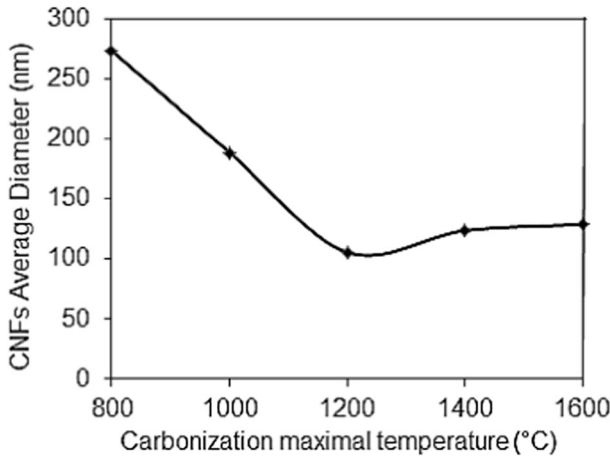
Fig. 6 Average diameter of carbonized CNFs as a function of carbonization maximum temperature

structure with increase of carbonization maximal temperature. For the nanofibers carbonized up to the temperatures above 1200 ˚C, it was reported a slight increment of the CNFs average diameter. Average diameter of the CNFs carbonized up to 800, 1000, 1200, 1400 and 1600 ˚C was recorded about 274, 189, 106, 124 and 129 nm, respectively. For the CNFs carbonized up to the temperatures above 1200 ˚C, it was not observed high decreasing in N and O contents but it was seen a considerable shrinkages on the fibers surface, resulted in slight increment of average diameter of the carbonized CNFs.

X-ray diffraction analysis (XRD) was used in order to determine of crystalline size or stacking height of the layer planes (L_c) and (002) interlayer d-spacing (d_{002}). The (002) peak is the more important peak in the XRD pattern of carbon materials, which is attributed to distance of the aromatic rings in the turbostratic and polyaromatic alternating layers [23, 24]. Hence, d_{002} and L_c were calculated using Bragg's law (Eq. 2) and Deby-Scherrer formula (Eq. 3), respectively [24, 25].

$$d_{002}(\text{nm}) = \frac{\lambda}{2.\text{Sin}\theta} \tag{2}$$

$$L_c(\text{nm}) = \frac{K.\lambda}{\beta.\cos\theta} \tag{3}$$

where K is the Scherrer parameter usually taken as 0.94 for (002) diffraction trace [26], λ is the wavelength of the X-ray source from Cu (0.154 nm), β is the full width at half maximum intensity in radians and θ is the diffracted angle belong to the diffraction trace of (002) planes. Figure 7 shows the XRD diffraction patterns of the CNFs carbonized up to 800–1600 °C in the scattering region of $2\theta = 10-40°$. For the carbonized CNFs, the peak appeared in the region of $2\theta = 25.91 - 27.01°$ is

Fig. 7 XRD diffraction patterns of PAN-based CNFs carbonized up to different maximum temperatures (800–1600 °C) in the scattering region of $2\theta = 10 - 40°$
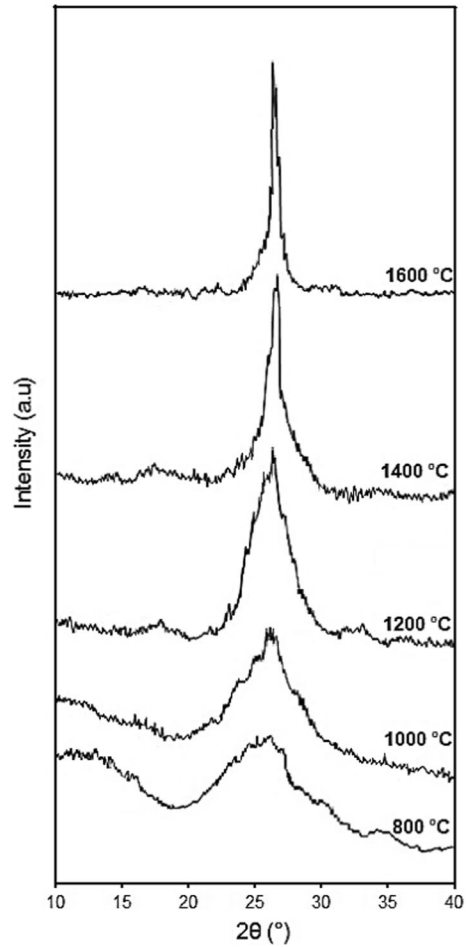

Table 4 Analysis of X-ray diffraction traces of PAN-based CNFs as a function of carbonization maximum temperature

| T_{max} (°C)	$2\theta_{002}$ (°)	d_{002} (nm)	β(°)	β(Radians)	Lc (nm)	Number of graphene layers (L_c/d_{002})
800	25.91	0.206	9.97	0.174	0.897	4.35
1000	25.91	0.206	7.61	0.133	1.175	5.71
1200	26.67	0.115	4.23	0.074	2.640	22.96
1400	27/01	0.096	2.19	0.038	6.366	66.31
1600	26.49	0.130	1.04	0.018	9.896	76.12

attributed to the (002) diffraction. For the CNFs carbonized up to the temperatures below 1200 °C, the wider root of the (002) diffraction trace confirms the characteristics of the disordered graphite-like sheets and turbostratic structure. With rising T_{max} from 800 to 1600 °C, the peak attributed to (002) diffraction increased in intensity and became sharper, that confirms the developing polyaromatic structure. The samples structural parameters obtained from (002) diffraction trace are listed in Table 4. As seen in this table, with increase of T_{max} from 800 to 1000 °C, the position of the peak was unchanged indicating the constant value of the interlayer d-spacing (d_{002}). Position of the peak moved to higher angles with rising T_{max} from 1000 to1400 °C, indicating the reduction in d_{002}. With the more increase of T_{max}; rising to 1600 °C, interlayer d-spacing of (002) was increased again (Fig. 8). It seems due to the formation of considerable shrinkages and voids in the CNFs structure.

The crystalline size (L_c) of the CNFs was presented in Fig. 8. This figure demonstrates the continuous increment of L_c with increase T_{max} from 800 to 1600 °C. As seen in this figure, the main increment of L_c has been occurred at the maximum temperatures above 1200 °C, which indicates the beginning of graphitization. The number of graphene layers could be calculated by L_c/d_{002}. Increasing the L_c/d_{002} with rising T_{max}, corresponds to an increase of the graphene layers in single crystallite that confirms developing the polyaromatic structure (Table 4). The low value of the L_c/d_{002} at the temperatures below 1200 °C confirms the low developing rate of polyaromatic structure.

In-plane graphitic crystallite size (L_a) of the samples was studied using Raman spectra. Raman spectroscopy can determine the L_a and structural characterization in a carbonaceous material, based on the study of two frequency bands (D and G bands) that characterize the majority of carbon materials such as CNFs and CNTs (carbon nanotubes) [27]. In-plane graphitic crystallite size (L_a) was calculated according to the Eq. (4) developed by Knight and White, where I_D and I_G are the intensity of D and G bands from Raman spectrum [28].
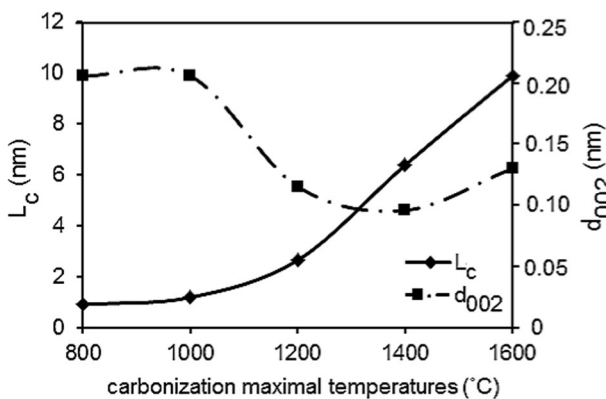
Fig. 8 Crystalline stacking thickness or crystalline size (Lc) and interlayer d-spacing (d_{002}) of carbonized CNFs as a function of carbonization maximum temperature
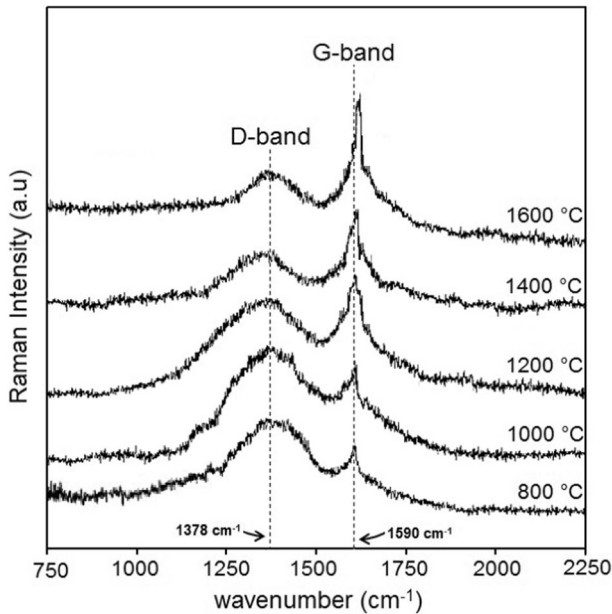
**Fig. 9** Raman spectra of PAN-based CNFs carbonized up to different maximal temperatures (800–1600 °C)

$$L_a(nm) = 4.4\left(\frac{I_D}{I_G}\right)^{-1} \tag{4}$$

Figure 9 shows the representative Raman spectra of the CNFs carbonized up to the different maximal temperatures. The peak appeared in the range of 1378–1386 cm^{-1} attributed to the D-band, indicating the presence of disordered sp^3 carbon structure and turbostratic structure of CNFs. Another prominent peak (G-band) was observed in the region of 1590–1601 cm^{-1}, which was assigned to C=C (sp^2) bond stretching vibrations, representing the more ordered polyaromatic structure of CNFs [27]. I_D/I_G ratio and L_a value calculated from the samples Raman spectra are listed in Table 5.

Table 5 Analysis of Raman spectra obtained from the PAN-based CNFs as a function of carbonization maximal temperature

| T_{max} (°C)	D Peak position (cm^{-1})	G Peak position (cm^{-1})	I_D/I_G	La (nm)
800	1378	1590	1.33	3.40
1000	1380	1592	1.08	4.07
1200	1380	1595	0.57	7.69
1400	1384	1596	0.49	8.89
1600	1386	1601	0.21	20.96
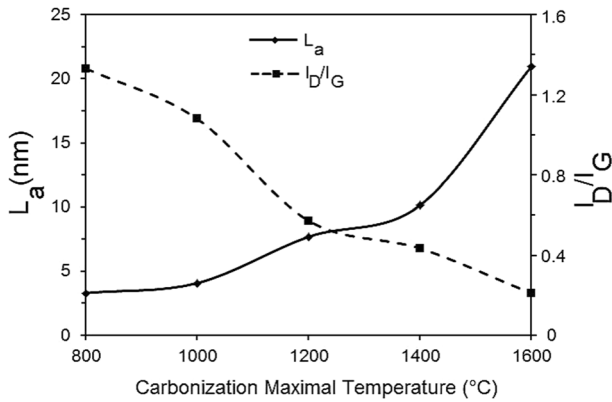
Fig. 10 In-plane graphitic crystallite size (L_a) and I_D/I_G ratio for the carbonized PAN-based CNFs as a function of carbonization maximum temperature

It is clear from this table that L_a value has been continuously increased with increase T_{max}, which is presented in Fig. 10. There is an inverse relationship between L_a and I_D/I_G ratio. Therefore, the ratio of D-band intensity to G-band intensity (I_D/I_G) has been continuously decreased with increasing T_{max}. As seen in this figure, for the CNFs carbonized up to temperature below 1000 °C, $I_D/I_G > 1$ that means the intensity of D peak is bigger than that of G peak, which indicates that the content of carbon bonds in the form of polyaromatic structure (graphite structure) is relatively lesser than carbon bonds in the form of disorder turbostratic structure. When T_{max} was increased to the temperatures above 1000 °C, $I_D/I_G < 1$ that means the intensity of G peak is bigger than that of D peak, which indicates that the most of carbon atoms exist in the form of polyaromatic structure, and the microstructure tends to be in order.

It is also clear from the Raman spectra that the peaks have been shifted to higher wavenumber (blue shift) with increasing T_{max}. Blue and redshifts of Raman peaks are related to the corresponding chemical bond length. The shorter bond length causes to shift the peaks to higher wavenumber or vice versa [29]. While the D-band generally indicates the existence of six-fold aromatic rings, the G-Band due to any in-plane bond stretching of two sp^2 carbons (C=C) [30]. Decreasing the I_D/I_G ratio with increasing of T_{max} represents developing the in-plane C=C bonds in the CNFs structure [31]. Double bonds involving carbon are stronger than single bonds and are also shorter [32]. Therefore, developing the CNFs in-plane C=C bonds can cause to minor shift the peaks to higher wavenumber.

There is a certain relationship between L_a and the nearest neighbor carbon–carbon distance named interatomic distances (R_{C-C}). Figure 11a shows a graphite-like structure in which the carbon atoms are linked by covalent bonds. The interatomic distances (R_{C-C}) presented in this figure can be calculated by Eq. 5 [33, 34], where P is the layer dimension parameter (Fig. 11b). P is calculated using Eq. (6), which La is the samples in-plane graphitic crystallite size listed in Table 5.
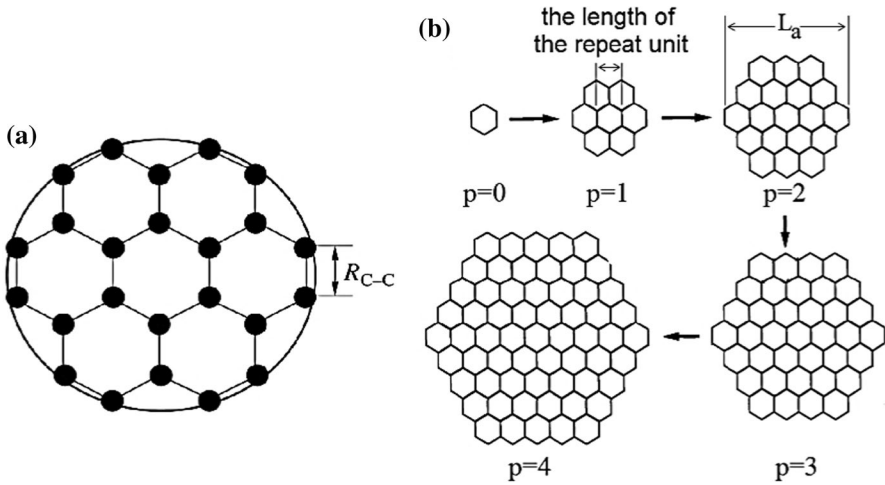
Fig. 11 Schematic of a graphite layer for a carbon material: structure of an individual graphite layer (**a**), a graphite layer when P varies from 0 to 3 [33, 34]
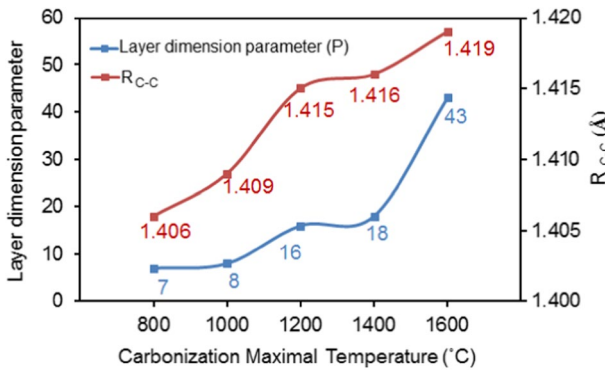
Fig. 12 Interatomic distances (R_{C-C}) and the layer dimension parameter (P) as a function of CNFs carbonization maximum temperature

$$L_a = 2R_{C-C}\cos30(2P - 1) \qquad (5)$$

$$L_a = \left(0.246 - \frac{0.020}{P}\right)(2P - 1) \qquad (6)$$

As seen in Fig. 12, R_{C-C} and P have been continuously increased by increase of CNFs carbonization maximum temperature, which is due to the increase of bond order [33]. The ratio of D-band intensity to G-band intensity (I_D/I_G) is decreased by increase of La. This feature indicates that the content of carbon atoms in the

form of polyaromatic structure increased by increase of La, which has been led to creation of more order bonds of carbon atoms.

In order to calculate the specific volume of Lennard–Jones potential by Eq. (1), it is necessary to find the depth of the Lennard–Jones potential (ε) and carbon particles volume (v_0). It has been proved that the Lennard–Jones parameters will change with hybridization, but this change will be little as compared to the geometric change in the molecule after changing the bonding. CNFs microstructure is mainly constructed of phenolic rings by hybridization of SP^3 and SP^2. According to the data recorded by W. L. Jorgensen [35], the average value of ε for the atomic pair of C–C in the C–OH phenol groups is 0.070 kcal mol^{-1} [Table 1 in reference 36]. Carbon particles volume in the samples (v_0) is calculated by $v_0 = d^3$ (d is the diameter of carbon atoms). As seen in Fig. 11a, the diameter of carbon atoms (d) is approximately equal to the nearest neighbor carbon–carbon distance ($d \cong R_{C-C}$). Table 6 shows the values of R_{C-C} and v_0 of the samples carbonized up to various temperatures. It is clear from this table that v_0 has been slightly increased by increase of carbonization maximum temperature. Therefore, the specific volume at the minimum distance of Lennard–Jones potential increased with increase of carbonization maximum temperature (Fig. 13a). It is also clear from this figure that the specific volume of the all samples has been continuously increased by increasing of temperature.
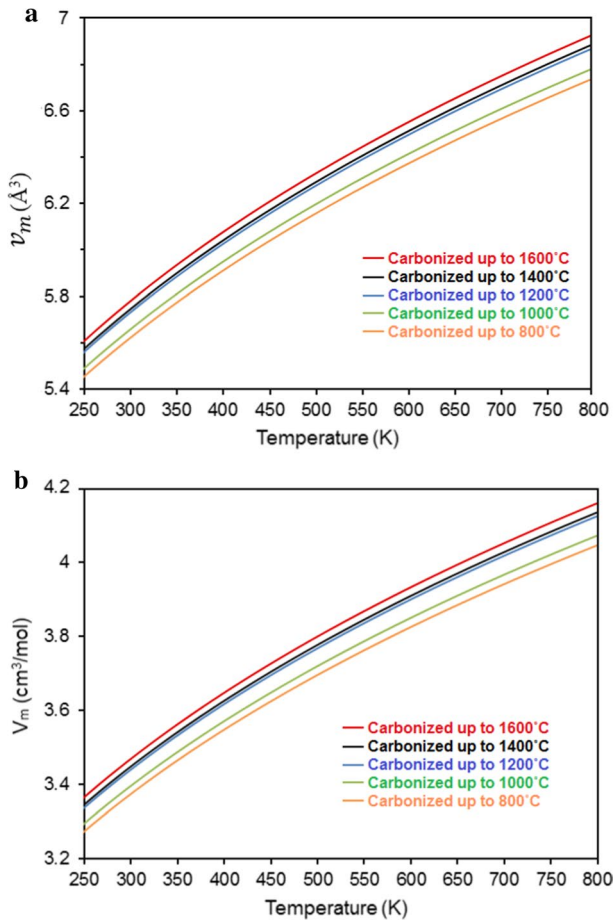
Molar specific volume of Lennard–Jones potential (V_m) was calculated by equation of (7), where N_A is Avogadro number (v_m is in the unit of Å^3). According to this equation, the molar specific volume depends on v_m and therefore temperature. Figure 13b shows the molar specific volume of the samples as a function of temperature. V_m has been increased with increase of carbonization maximum temperature. It is also clear from this figure that for the various temperatures, the molar specific volume has been increased by increase of the CNFs carbonization maximum temperature. Molar specific volume at the ambient temperature (~300 K) was recorded about 3.374, 3.396, 3.440, 3.448 and 3.469 cm^3/mol for the samples carbonized up to 800, 1000, 1200, 1400 and 1600 °C, respectively.

$$V_m \left(cm^3/mol \right) = N_A v_m \times 10^{-24} \tag{7}$$

Figure 14a shows the results N_2 adsorption isotherms of carbonized PAN-based CNF webs. The results are also listed in Table 7. It is clear from this table and Fig. 14b that the surface area and pore volume are significantly influenced by the carbonization maximum temperature. The specific surface area (S_{BET}) of the CNFs has been continuously increased from 124 m^2.g^{-1} to 544 m^2.g^{-1} by increasing T_{max}

| Table 6 In-plane graphitic crystallite size (La), interatomic distances (R_{C-C}) and carbon particles volume (v_0) of the CNFs carbonized up to the various temperature	T_{max} (°C)	La (nm)	P	R_{C-C} (Å)	v_0 (Å^3)
	800	3.40	7	1.406	2.779
	1000	4.07	8	1.409	2.797
	1200	7.69	16	1.415	2.833
	1400	8.89	18	1.416	2.839
	1600	20.96	43	1.419	2.857

Fig. 13 Specific volume of CNFs: **a** at which Lennard–Jones potential reaches its minimum value (v_m), **b** defined for 1 mol CNFs (V_m)

from 800 °C to 1600 °C. Pore total volume has been increased from 0.15 $cm^3.g^{-1}$ to 0.48 $cm^3.g^{-1}$ by increasing T_{max} from 800 °C to 1600 °C.

It is also clear from Table 6 that T_{max} of 800 °C, 1200 °C and 1400 °C resulted in low mesopore volume (< 0.2 $cm^3.g^{-1}$), which is related to creation of small size pores. It has been reported that the large pores could destructively affect the mechanical properties, thermal expansion and oxidative stability of CNFs and diamond-like materials [36]. It has been also confirmed that the mechanical properties of CNFs can be increased by increase of the arrangement level in CNFs turbostratic microstructure [37]. According to Raman spectra represented in Fig. 9 and Table 5, the microcrystalline structure of the sample became more rearranged by increasing of T_{max}. Increasing of the arrangement degree of the turbostratic structure is related to decrease of the amount of defective carbon structures, which can lead to synthesize of more strong CNFs [3]**.** Therefore, it
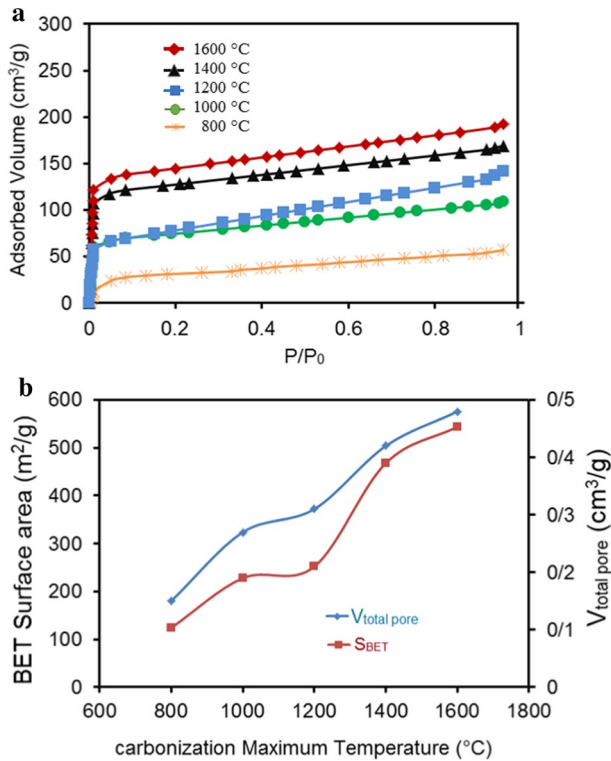
Fig. 14 N_2 adsorption isotherms graph of the CNFs carbonized up to various Tmax (**a**), BET surface areas and total pore volume as a function of the Tmax

Table 7 Porosity analysis of CNFs after carbonization up to various T_{max}

T_{max} (°C)	S_{BET} ($m^2 \cdot g^{-1}$)	V_{total} ($cm^3 \cdot g^{-1}$)	V_{meso} ($cm^3 \cdot g^{-1}$)	V_{micro} ($cm^3 \cdot g^{-1}$)
800	124	0.15	0.12	0.03
1000	228	0.27	0.24	0.03
1200	252	0.32	0.16	0.16
1400	468	0.42	0.14	0.28
1600	544	0.48	0.37	0.11

is expected that T_{max} of 1200–1400 °C leads to synthesize of more strong CNFs because of low mesopore volume and high ordered microstructure. Carbonization at 800 °C is not suggested because of high value of I_D/I_G ratio and subsequently low arrangement of carbon atoms. Also, carbonization at 1000 °C and 1600 °C is not suggested because of high value of mesopores volume. To verify this matter, tensile test was performed for all samples. Figure 15 shows stress–strain curves of the CNFs mats carbonized up to various temperatures of 800–1600 °C. The mechanical properties obtained from stress–strain curves of CNFs mats are listed
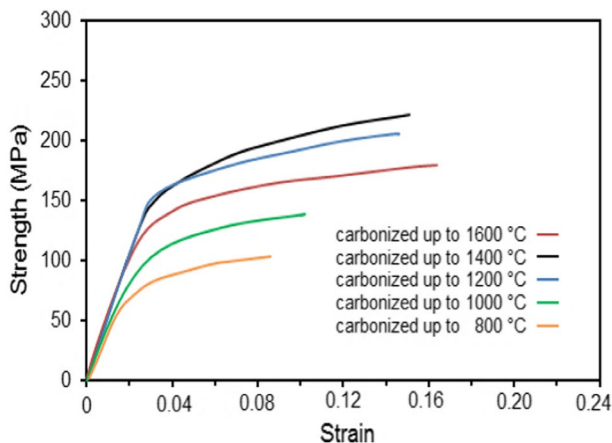
Fig. 15 Stress–strain curves of PAN-based CNFs mats carbonized up to different maximum temperatures (800–1600 °C)

Table 8 Analysis of stress–strain curves obtained from carbonized PAN-based CNFs as a function of carbonization maximum temperature

T_{max} (°C)	Yield stress (MPa)	Tensile strength (MPa)	Fracture strain	Yield strain	Young's modulus (MPa)
800	65	103	0.162	0.015	4333
1000	87	142	0.150	0.020	4550
1200	149	206	0.146	0.031	4806
1400	142	223	0.103	0.029	4897
1600	123	179	0.086	0.025	4920

in Table 8. As seen in this table and Fig. 16a, tensile strength of the CNFs mat increased with rising T_{max} from 800 to 1400 °C, which related to the decrease of CNFs average diameter and also increase of the Lc and La. The highest value of the tensile strength was recorded 223 MPa belongs to the CNFs mat carbonized up to the 1400 °C. Tensile strength of the CNFs mat carbonized up to the 1600 °C was recorded 179 MPa, which is 44 MPa less than that belongs to the sample carbonized up to the 1400 °C. This is most probably caused by increase of d_{002} (0.130 nm) and mesopore volume (0.37 $cm^3.g^{-1}$). Carbon atoms distance in the alternating graphene layers has been increased with increase the interlayer d-spacing (d_{002}), which resulted in decreasing the link strength of carbon atoms in the alternating graphene layers.

It is also clear from Fig. 16b that young's modulus (E) of the CNFs mat has been continuously increased with increase of T_{max} from 800 to 1600 °C, which is due to the increase the number of graphene layers in each crystallite. The highest value of E was recorded 4920 MPa for the CNFs mats carbonized up to 1600 °C,
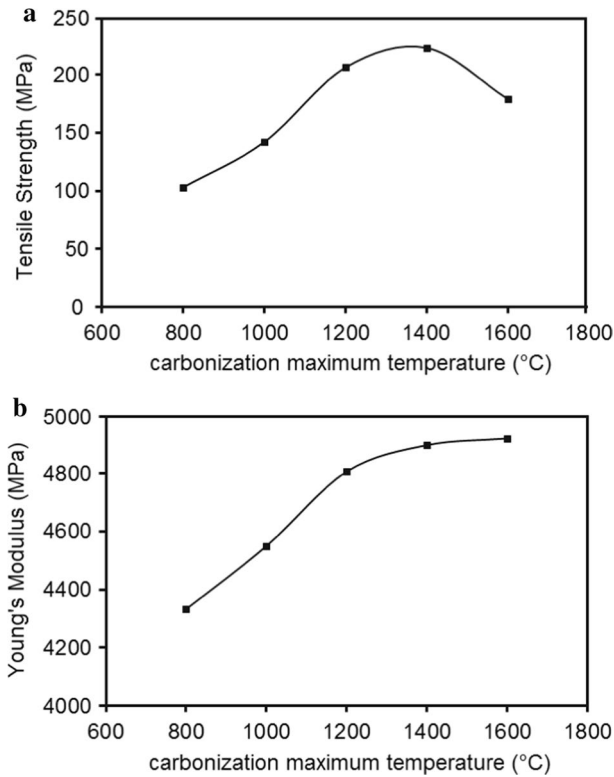
Fig. 16 Tensile strength (**a**), and Young's modulus (**b**) of the carbonized CNFs mats as a function of carbonization maximum temperature

that is approximately same as that recorded to the samples carbonized up to 1400 °C (4897 MPa) and 1200 °C (4806 MPa).

Poisson ratio of the samples was calculated using Eq. (8) developed by J.T. Seitz [38], where A is the molecular cross-sectional area. A can be calculated by formula of (9), which V_ω is the molar volume, l_m is the length of the repeat unit in its fully extended conformation and N_A is Avogadro's number.

$$v = -2.37 \times 10^6 \sqrt{A} + 0.513 \tag{8}$$

$$A = \frac{V_\omega}{N_A l_m} \tag{9}$$

We considered the value of La/2P + 1 (Fig. 11b) as the length of the repeat unit ($l_m \cong \frac{L_a}{2P+1}$) and the Lennard–Jones molar specific volume as the molar volume ($V_\omega = V_m$). Lennard–Jones molar specific volume and the molar volume are close to each other and agree well with each other [20]. As previously seen in Fig. 13, Lennard–Jones specific volume varies by temperature and therefore, Poisson ratio
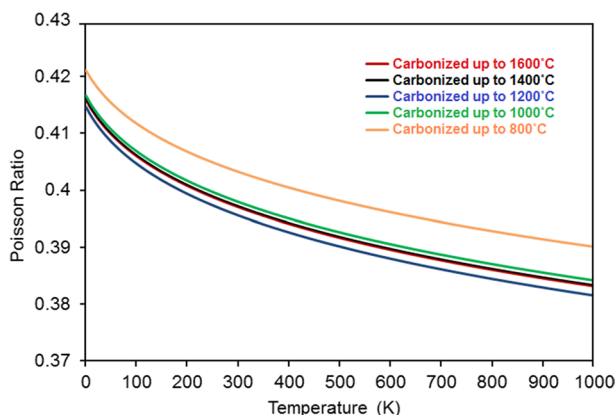
Fig. 17 Poisson ratio of the CNFs samples as a function of temperature

will be vary by temperature. Figure 17 shows the samples Poisson ratio as the function of temperature. As seen in this figure, Poisson ratio of the all samples has been continuously decreased by increase of temperature. At the various temperatures, maximum value of Poisson ratio was recorded for the CNFs carbonized up to 800 ˚C. Also, Minimum value of Poisson ratio was recorded for the CNFs carbonized up to 1200 ˚C. Poisson ratio at the ambient temperature (~ 300 K) was recorded about 0.403, 0.399, 0.395, 0.397 and 0.397 for the samples carbonized up to 800, 1000, 1200, 1400 and 1600 ˚C, respectively. These values are close to the Poisson ratio values recorded for armchair CNTs [39].

Based on the main structural and mechanical properties of the samples summarized in Table 9, it seems that carbonization CNFs up to temperature in the range of 1200–1400 °C is more efficient to creation of PAN-based carbon nanofibers mats with high number of the strong graphene layers and high mechanical properties.

Table 9 Structural and mechanical properties of the carbonized PAN-based CNFs mats as a function of carbonization maximum temperature

T_{max} (°C)	C (%wt.)	CNFs average diameter (nm)	d_{002} (nm)	L_c (nm)	L_a (nm)	Number of graphene layer	Y.S (MPa)	Tensile strength (MPa)	E (MPa)
800	79.42	274	0.206	0.897	3.40	4.35	65	103	4333
1000	85.68	189	0.206	1.175	4.48	5.71	87	142	4550
1200	90.53	106	0.115	2.640	7.69	22.96	149	206	4806
1400	91.75	124	0.096	6.366	8.89	66.31	142	223	4897
1600	92.87	129	0.130	9.896	20.96	76.12	123	179	4920

Conclusion

The effect of the carbonization maximum temperature (T_{max}) on the PAN-based carbon nanofibers physical and mechanical properties has been studied using SEM, BET, XRD, Raman and FTIR spectroscopies. XRD results showed that rising T_{max} from 800 to 1400 °C resulted in the increase of 2θ position and decrease of d_{002}. With the more rising of T_{max} (rising to 1600 °C), d_{002} was increased again, perhaps due to the formation of considerable mesopores in the CNFs structure. Raman spectra showed that the in-plane graphitic crystallite size (La) continuously increased with rising T_{max}, which is related to the developing more ordered polyaromatic structure. It was also observed a blue shift of Raman D and G-band with increasing T_{max} because of the developing in-plane shorter carbon bonds ($C=C$). It was clear from the results of N_2 adsorption isotherms that the specific surface area (S_{BET}) and pore total volume increased by increasing T_{max} from 800 °C to 1600 °C. Tensile strength of the CNFs mat continuously increased (from 103 to 223 MPa) with rising Tmax from 800 °C to 1400 °C, which corresponds to the decrease of CNFs average diameter and also increase of the Lc and La. Tensile strength of the sample carbonized up to the 1600 °C (179 MPa) was recorded 44 MPa less than that belongs to the sample carbonized up to the 1400 °C. This is most probably caused by the increase of mesopore volume (0.37 $cm^3.g^{-1}$). Therefore, T_{max} of 1200–1400 °C was recognized more efficient because of synthesis of more strong CNFs with high ordered low porous structure.

Compliance with ethical standards

Conflict of interests The authors declare that they have no conflict of interest.

References

1. Figueiredo JL, Bernardo CA, Baker RTK, Huttinger KJ (1990) Carbon fibers filaments and composites, 2nd edn. Kluwer academic publishers, Portugal
2. Li D (2004) Electrospinning of nanofibers: reinventing the wheel. Adv Mater 16:1151–1170. https://doi.org/10.1002/adma.200400719
3. Marcuzzo JS, Otani C, Aguiar Polidoro H, Otani S (2013) Influence of thermal treatment on porosity formation on carbon fiber from textile PAN. Mater Res 16:137–144. https://doi.org/10.1590/S1516-14392012005000165
4. Inagaki M, Yang Y, Kang F (2012) Carbon nanofibers prepared via electrospinning. Adv Mater 24:2547–2566. https://doi.org/10.1002/adma.201104940
5. Newcomb BA (2016) Processing, structure, and properties of carbon fibers. Compos Part A Appl Sci Manuf 91:262–282. https://doi.org/10.1016/j.compositesa.2016.10.018
6. Cai J, Li W, Zhao P, Yu J, Yang Z (2018) Low-cost and high-performance electrospun carbon nanofiber film anodes. Int J Electrochem Sci 13:2934–2944

7. Sutasinpromprae J, Jitjaicham S, Nithitanakul M, Meechaisue C, Supaphol P (2006) Preparation and characterization of ultrafine electrospun polyacrylonitrile fibers and their subsequent pyrolysis to carbon fibers. Polym Int 55:825–833. https://doi.org/10.1002/pi.2040

8. Park SH, Kim C, Yang KS (2004) Preparation of carbonized fiber web from electrospinning of isotropic pitch. Synth Met 143:175–179. https://doi.org/10.1016/j.synthmet.2003.11.006

9. Gu SY, Wu Q, Ren J (2008) Preparation and surface structures of carbon nanofibers produced from electrospun PAN precursors. New Carbon Mater 23:171–176. https://doi.org/10.1016/S1872-5805(08)60021-9

10. Sadighzadeh A, Valinejad M, Gazmeh A, Rezaiefard B (2016) Synthesis of Polymeric electrospun nanofibers for application in waterproof-breathable fbrics. Polym Eng Sci 1:143–149. https://doi.org/10.1002/pen.24200

11. Rajalingam P, Radhakrishnan G (1991) Polyacrylonitrile precursor for carbon fibers. JMS-REV Macromol Chem Phys C 31:301–310. https://doi.org/10.1080/15321799108021925

12. Rahaman MSA, Ismail AF, Mustafa A (2007) A review of heat treatment on polyacrylonitrile fiber. Polym Degrad Stab 92:1421–1432. https://doi.org/10.1016/j.polymdegradstab.2007.03.023

13. Ko TH, Day TC, Lin MF (1993) The effect of precarbonization on mechanical properties of final polyacrylonitrile-based carbon fibres. J Mater Sci Lett 12:343–345. https://doi.org/10.1007/BF01910099

14. Cohn SM, Das S(1998) A cost assessment of conventional PAN carbon fiber production technology, Energy division, Oak Ridge National laboratory, Tennessee, Unpublished draft

15. Deurbergue A, Oberlin A (1991) Stabilization and carbonization of pan-based carbon fibers as related to mechanical properties. Carbon 29:621–628. https://doi.org/10.1016/0008-6223(91)90129-7

16. Kostikov VI (1995) Fibre science and technology, 1st edn. Chapman and hall english, Netherland

17. Kim C, Park SH, Cho JI, Lee DY, Park TJ, Lee WJ, Yang KS (2004) Raman spectroscopic evaluation of polyacrylonitrile-based carbon nanofibers prepared by electrospinning. Raman Spectrosc 35:928–933. https://doi.org/10.1002/jrs.1233

18. Fitzer E, Frohs W, Heine M (1986) Optimization of stabilization and carbonization treatment of pan fibers and structural characterization of the resulting carbon fibers. Carbon 24:387–395. https://doi.org/10.1016/0008-6223(86)90257-5

19. Laffont L, Monthioux M, Serin V, Mathur RB, Guimon C, Guimon MF (2004) An EELS study of the structural and chemical transformation of PAN polymer to solid carbon. Carbon 42:2485–2494. https://doi.org/10.1016/j.carbon.2004.04.043

20. Al-Raeei M, El-Daher MS (2020) Temperature dependence of the specific volume of Lennard-Jones potential and applying in case of polymers and other materials. Polym Bull. https://doi.org/10.1007/s00289-020-03166-8

21. Brunauer S, Emmett PH, Teller E (1938) Adsorption of gases in multimolecular layers. J Am Chem Soc 60:309. https://doi.org/10.1021/ja01269a023

22. Zeng K, Minh DP, Gauthier D, Hortala EW, Nzihou A, Flamant G (2015) The effect of temperature and heating rate on char properties obtained from solar pyrolysis of beech wood. Biores Technol 182:114–119. https://doi.org/10.1016/j.biortech.2015.01.112

23. Bakar SSS, Foong KM, Halif NA, Yahud S (2019) Effect of solution concentration and applied voltage on electrospun polyacrylonitrile fibers. Mater Sci Eng 701:1–7. https://doi.org/10.1088/1757-899X/701/1/012018

24. Zhou G, Yu S, He L, Guo Q, Ye H (2012) The interpretation of X-ray diffraction from the pyrocarbon in carbon/carbon composites with comparison of TEM observations. Phil Mag 92:1198–1211. https://doi.org/10.1080/14786435.2011.640293

25. Warren BE (1941) X-Ray diffraction in random layer lattices. Phys Rev 59:693–698. https://doi.org/10.1103/PhysRev.59.693

26. Biscoe J, Warren BE (1942) An x-ray study of carbon black. J Appl Phys 13:364–371. https://doi.org/10.1063/1.1714879

27. Jorio A, Filho AGS (2016) Raman studies of carbon nanostructures. Annu Rev Mater Res 46:357–382. https://doi.org/10.1146/annurev-matsci-070115-032140

28. Knight DS, White WB (1989) Characterization of diamond films by Raman spectroscopy. J Mater Res 4:385–393. https://doi.org/10.1557/JMR.1989.0385

29. Bokobza L, Bruneel JL, Couzi M (2015) Raman spectra of carbon-based materials (from graphite to carbon black) and of some silicone composites. C-J Carbon Res 1:77–94. https://doi.org/10.3390/c1010077

30. Ferrari AC, Robertson J (2000) Interpretation of Raman spectra of disordered and amorphous carbon. Phys Rev B 61:14095–14107. https://doi.org/10.1103/PhysRevB.61.14095
31. Qanati MV, Rasooli A (2020) Functionalization of CNFs via wet chemical oxidation method in order to improve CNFs adhesion to matrix of carbon composites. Diam Relat Mater 109:1–9. https://doi.org/10.1016/j.diamond.2020.108097
32. Francis A, Sundberg A, Richard J (2007) Advanced organic chemistry carey, 5th ed, Springer US
33. Belenkov EA (2001) Formation of graphite structure in carbon crystallites. Inorg Mater 37:928–934. https://doi.org/10.1023/A:1011601915600
34. Fujimoto H, Mabuchi A, Tokumitsu K, Kasuh T (1994) Effect of crystallite size on the chemical compositions of the stage 1 alkali metal-graphite intercalation compounds. Carbon 32:193–198. https://doi.org/10.1016/0008-6223(94)90182-1
35. Jorgensen WL (2004) BOSS: Biochemical and organic simulation system user's manual for UNIX, Linux, and windows, version 4.6, department of chemistry, Yale university
36. Belenkov EA, Brzhezinskaya MM, Greshnyakov VA (2017) Crystalline structure and properties of diamond-like materials. Nanosyst Phy Chem Math. https://doi.org/10.17586/2220-8054-2017-8-1-127-136
37. Sazali N (2019) The influence of carbonization temperature and heating rate towards carbon membrane performance: a review. J Adv Res Fluid Mech Therm Sci 62:151–158
38. Seitz JT (1993) The estimation of mechanical properties of polymers from molecular structure. J Appl Polym Sci 49:1331–1351. https://doi.org/10.1002/app.1993.070490802
39. Ávila AF, Lacerda GSR (2008) Molecular mechanics applied to single-walled carbon nanotubes. Mater Res 11:325–333. https://doi.org/10.1590/s1516-14392008000300016